A&A 496, 765–775 (2009)
DOI: 10.1051/0004-6361:200810005

Astronomy & Astrophysics

Nova-like cataclysmic variable TT Arietis

QPO behaviour coming back from positive superhumps⋆

Y. Kim[1,2], I. L. Andronov[3,4], S. M. Cha[1], L. L. Chinarova[4], and J. N. Yoon[1]

[1] University Observatory, Chungbuk National University, 361-763, Cheongju, Korea
[2] Institute for Basic Science Research, Chungbuk National University, 361-63, Korea
[3] Odessa National Maritime University, Mechnikov str., 34, 65029 Odessa, Ukraine
e-mail: tt_ari@ukr.net; bfcyg@mail.ru; uavso@pochta.ru; i_andronov@yahoo.com
[4] Astronomical Observatory, Odessa National University, T.G. Shevchenko Park, 65014 Odessa, Ukraine

Received 18 April 2008 / Accepted 1 October 2008

ABSTRACT

Aims. We study the variability of the nova-like cataclysmic variable TT Ari, on time-scales of between minutes and months.
Methods. The observations in the filter *R* were obtained at the 40-cm telescope of the Chungbuk National University (Korea), 51 observational runs cover 226 h. The table of individual observations is available electronically. In our analysis, we applied several methods: periodogram, wavelet, and scalegram analysis.
Results. TT Ari remained in a "negative superhump" state after its return from the "positive superhump" state, which lasted for 8 years. The ephemeris for 12 of the best pronounced minima is $T_{\rm min}$ = BJD 2 453 747.0700(47) + 0.132322(53)E. The phases of minima may reach 0.2, which reflects the non-eclipse nature of these minima. The quasi-periodic oscillations (QPO) are present with a mean "period" of 21.6 min and mean semi-amplitude of 36 mmag. This value is consistent with the range 15−25 min reported for previous "negative superhump" states and does not support the hypothesis of secular decrease in the QPO period. Either the period, or the semi-amplitude show significant night-to-night variations. According to the position at the two-parameter diagrams (i.e. diagrams of pairs of parameters: time, mean brightness of the system, brightness of the source of QPO, amplitude, and timescale of the QPOs), the interval of observations was divided into 5 parts, showing different characteristics: 1) the "pre-outburst" stage; 2) the "rise to outburst"; 3) "top of the outbursts"; 4) "post-outburst QPO" state; and 5) "slow brightening". The the QPO source was significantly brighter during the 10-day outburst, than during the preceding interval. However, after the outburst, the large brightness of the QPO source still existed for about 30 days, producing the stage "4". The diagram for $m_{\rm QPO}(\bar{m})$ exhibits two groups in the brightness range $10\overset{\rm m}{.}6-10\overset{\rm m}{.}8$, which correspond to larger and smaller amplitudes of the QPO. For the group "5" only, statistically significant correlations were found, for which, with increasing mean brightness, the period, amplitude, and brightness of the of QPO source also increase. The mean brightness at the "negative superhump state" varies within $10\overset{\rm m}{.}3-11\overset{\rm m}{.}2$, so the system is brighter than at the "positive superhump" ($11\overset{\rm m}{.}3$), therefore the "negative superhump" phenomenon may be interpreted by a larger accretion rate. The system is an excellent laboratory for studying processes resulting in variations on timescales of between seconds and decades and needs further monitoring at various states of activity.

Key words. stars: novae: cataclysmic variables – stars: variables: general – stars: binaries: general

1. Introduction

TT Ari is one of the brightest and most extensively studied nova-like cataclysmic variable (see e.g. monographs by Warner 1995; and Hellier 2001). A wide variety of processes occur in this object, making it variable at time scales from 9.6 s (Kozhevnikov 1986) to years (Hudec et al. 1984; Bianchini 1990; Kraicheva et al. 1999). Due to its low inclination, there were no prominent eclipses in the light curve, but there was a "negative superhump"-type modulation and ∼20-min quasi-periodic oscillations (QPO). Mardirossian et al. (1980) reported ∼$40^{\rm s}$ "oscillatory events", ≥6-min QPOs, flickering, and an almost sinusoidal shape of 3-h modulations.

Krautter et al. (1981) classified TT Ari as "a dwarf nova at a permanent outburst". Hoard (2007) included TT Ari as a part of his "Big list" of the SW Sex stars (see e.g. Hellier 2000, for a review). Semeniuk et al. (1987) identified 4 periods in TT Ari, namely, 3.8 day beat period of the 3.2-h photometric and 3.3 h spectroscopic periods, and quasi-periodic oscillations (QPO), and an apparent decrease in the QPO period from 27 (in 1961) to 17 min (in 1985). Kozhevnikov (1986) detected variability on a short timescale of 9.6 s.

To study these different types of variability, several international observational campaigns were organized, the results of which were summarized by Wenzel et al. (1986), Tremko et al. (1996), Skillman et al. (1998) and Andronov et al. (1999). Hollander & van Paradijs (1992) proposed a dependence of QPO characteristics on accretion rate. Kraicheva et al. (1999) and Stanishev et al. (2001) suggested variations in the accretion rate as a cause of switches between the positive and negative superhumps, and reported that in the positive superhump state the

⋆ Table 2 is only available in electronic form at the CDS via anonymous ftp to cdsarc.u-strasbg.fr (130.79.128.5) or via http://cdsweb.u-strasbg.fr/cgi-bin/qcat?J/A+A/496/765

flickering amplitude is smaller than in the brighter superhump state.

One of the most exciting events in TT Ari was a switching in 1997 from the state of "negative" superhumps, which lasted for almost 3 decades of optical studies, to a state of "positive" superhumps (Skillman et al. 1998), in excellent agreement with the "$P_{\rm orb} - P_{\rm sh}$" ("orbital period – superhump period") statistical relation (Andronov et al. 1999). The system exhibited highly asymmetric ($M - m = 0.320(5)$) permanent superhumps of a similar amplitude of $0\overset{\rm m}{.}19$ in both V and R and a period of $0\overset{\rm d}{.}14841(1)$ in 2004 (Andronov et al. 2005). However, in 2005, the system reverted state to negative superhumps with possibly some additional evidence for instability (Andronov et al. 2005). This event initiated regular photometric monitoring at the Chungbuk National University. Preliminary results were published briefly by Yoon et al. (2006). Results of the observational campaign are presented in this paper.

2. Observations and comparison stars

2.1. Observations

The time-series observations in R band were acquired using a 512×512 FLI CM-1 CCD mounted on the 40 cm telescope at Chungbuk National University (MAEDE LX200). The field of view of a CCD image is about 12.97×12.97 arcmin^2, given a CCD plate scale of $1\overset{''}{.}52$ per pixel at the $f/6.3$ Schmidt-Cassegrain focus of the telescope.

Instrumental signatures of each CCD frame were removed and calibrated using the bias, dark, and flat field frames, with the aid of the IRAF package CCDRED. We obtained instrumental magnitudes of stars from the empirical point-spread function (PSF) fitting method in the IRAF package DAOPHOT (Stetson 1987; Massey & Davis 1992).

The journal of observations is presented in Table 1. All Julian dates are expressed by omitting "24" at the beginning, so that the integer part contains 5 digits instead of 7. For the legend of a separate night of observations, we used the integer "legend Julian Date" LJD = int(BJD$_1$ − 0.5), where BJD is barycentric Julian date, BJD$_1$ is BJD for the first observation, and int(x) is an integer part of x. An additional substraction of 0.5 was required because the integer part of BJD changed many runs during the night. This method prevents duplication of LJD for different runs, for example, the run starting on 53 684.04 will have a designation LJD = 53 683, whereas the next run starts at 53 684.97 (LJD = 53 684). Therefore, BJD–LJD represents elapsed time in days with respect to the legend Julian date, and may exceed unity. For all observational runs, BJD–LJD ranged between 0.88 and 1.34, corresponding to 14 199 observations obtained during 226 h in 51 nights (JD 2 453 669-2 453 800).

The original observations (BJD, R magnitude) are presented in Table 2. For two nights, there was CCD V photometry (one night a series of V, and another night sequences $VRVR$... with alternatively changing filters).

2.2. Comparison stars

The photometric UBV standards in the field have been published by Goetz (1985). His photometric data was calibrated on to a standard scale by comparing the brightness of the star "c" (=GSC 1207 1535) measured by him and by Shafter et al. (1985). The chart based on Hipparcos and Tycho catalogues is also presented by the VSNET (2005) in B and V. The $UBVRI$ magnitudes were published for only one star "c", and were determined by Efimov et al. (1998) by linking to the standard star HD 23 949 (Neckel & Chini 1980). The check star "d" (=GSC 1207 1562), which is closer to TT Ari and more suitable for measurements, is much redder ($B - V = 1\overset{\rm m}{.}15$) than "c" ($B - V = 0\overset{\rm m}{.}69$) (Goetz 1985). Taking into account, that the color index of "c" is closer to that of the variable, than that of "d", it is recommended to use "c" as the comparison star.

Henden (2007) published $BVRI$ magnitudes for many stars in the field, including "c" ($V = 11\overset{\rm m}{.}05$, $R = 10\overset{\rm m}{.}66$) and "d". A compilation of magnitude estimates is presented in Table 3. The difference between the brightness estimates for the comparison star "c" in the filter R reaches $0\overset{\rm m}{.}25$. This value is typical of discrepancies between "standard" stellar magnitudes determined by different authors. Finally, for the calibration of our observations, we adopted the values ($V = 11\overset{\rm m}{.}01$, $R = 10\overset{\rm m}{.}41$) published by Efimov et al. (1998). No color correction was derived, so the instrumental magnitudes were defined to be the adopted brightness of the comparison star plus instrumental difference "variable-comparison". The error estimates for a single measurement of the variable varied between $0\overset{\rm m}{.}008$ (for the night at the top of the outburst) and $0\overset{\rm m}{.}026$ (for 6 nights in the faint state).

3. Results of analysis of multi-component variability

3.1. Light curves

The multi-type nature of the variability has been reported by previous researches. In this work, we complete a time series analysis of unprecedented number of observational runs, which were obtained in the same instrumental photometric system R. Only 1 night was obtained using another filter – V. The complete light curve, obtained during the present observational campaign, is shown in Fig. 1. According to the nature of the variability and values of the mean brightness $\bar{m}$ in Table 1, it may be divided into several subintervals:

- 53 668–53 700: $\bar{m}$ ranged from $11\overset{\rm m}{.}00$ to $11\overset{\rm m}{.}18$, and this may be characterized as the "pre-outburst" stage. However, we can discern a slow brightening from 52 682 to 53 700 with a best-fit function slope of $\dot{m} = {\rm d}m/{\rm d}t = -0.00624(19)$ mag/day. Hereafter, the numbers in brackets indicate the error estimate in units of the last digit. Another important characteristic of outbursts is a "decay time" $T_{\rm decay} = {\rm d}t/{\rm d}m$ for the descending branch of the outburst (cf. Bailey 1975; Warner 1995), and, similarly, a "rise time". $T_{\rm rise} = -{\rm d}t/{\rm d}m$ for the ascending branch. According to the properties of the least-square linear fits, $|\dot{m}T_{\rm rise}| = \rho^2$, where ρ is the correlation coefficient between time t and brightness m. For this time interval of our observations, $T_{\rm rise} = 37.0 \pm 1.1$ days/mag.
- 53 700–53 714: "rise to the outburst", the star brightened from $\bar{m} = 11\overset{\rm m}{.}09$ to $10\overset{\rm m}{.}26$ in 14 days, $T_{\rm rise} = 16.0 \pm 0.1$ days/mag, and $\dot{m} = -0.0584(4)$. The slope at the ascending branch is a factor of 9.4 steeper than in the "pre-outburst" stage. The shape of the rise is noticeably linear, with a large correlation coefficient $\rho = -0.9668(65)$. The slope is lower than that for outburst of dwarf novae by an order of magnitude (cf. Warner 1995), which implies to a different nature (possibly an increase in the mass transfer rate).
- 53 712–53 721: "top of the outburst", two nights 53 712, 53 713 from 5 may belong both to the "rise" and "top", as the brightness continued to increase, whereas the values for these two nights are in an agreement to the range characteristic of the "top". The mean value is $\bar{m} = 10\overset{\rm m}{.}341(3)$.

Table 1. Journal of observations of TT Ari: The "legend Julian date LJD" (integer part of the Julian date for the beginning of the night); number of observations n; time of the begin t_b and end t_e of observations (for the many nights, the observations ended on the next integer JD); duration of the run $t_e - t_b$; magnitude range for individual data points m_{max}, m_{min}; nightly mean $\bar{m}$ and it's accuracy estimate $\sigma(\bar{m})$; rms deviation of the single observation from the mean $\sigma(m)$; exp – time resolution in seconds. All moments of time are expressed in (BJD-2 400 000).

LJD	n	$t_b - t_e$	Duration	Range	$\bar{m}$	$\sigma(\bar{m})$	$\sigma(m)$	Exp
53 668	89	53669.12931-69.20075	0.07144	10.847-11.167	10.9975	0.0073	0.0687	64
53 682	127	53683.16957-83.29230	0.12273	10.995-11.338	11.1820	0.0057	0.0641	77
53 683	243	53684.03965-84.24841	0.20876	11.045-11.289	11.1667	0.0033	0.0508	62
53 684	213	53684.97582-85.14497	0.16915	11.000-11.282	11.1341	0.0042	0.0613	53
53 685	326	53685.98716-86.29891	0.31175	10.997-11.288	11.1767	0.0028	0.0509	67
53 686	445	53686.91790-87.27436	0.35646	10.929-11.303	11.1435	0.0031	0.0646	58
53 691	545	53691.89585-92.26499	0.36914	10.986-11.256	11.1194	0.0021	0.0491	48
53 692	371	53692.94350-93.25535	0.31185	10.975-11.239	11.1228	0.0026	0.0494	53
53 693	302	53693.97067-94.27612	0.30545	10.982-11.268	11.1418	0.0029	0.0497	78
53 694	331	53694.98199-95.26401	0.28202	10.972-11.224	11.1039	0.0028	0.0506	68
53 696	326	53696.92302-97.16962	0.24660	10.962-11.252	11.1090	0.0028	0.0506	49
53 698	376	53698.88323-99.29020	0.40697	10.773-11.228	11.0404	0.0028	0.0548	54
53 700	38	53701.05339-01.09047	0.03708	10.956-11.180	11.0932	0.0075	0.0460	73
53 703	159	53704.14776-04.27062	0.12286	10.804-11.052	10.9180	0.0044	0.0561	57
53 704	216	53705.07537-05.24029	0.16492	10.712-10.959	10.8413	0.0035	0.0509	54
53 706	391	53707.03617-07.24017	0.20400	10.582-10.905	10.7678	0.0031	0.0605	34
53 707	31	53707.89166-07.92107	0.02941	10.660-10.885	10.7859	0.0106	0.0593	69
53 712	301	53713.00121-13.16906	0.16785	10.265-10.615	10.4350	0.0040	0.0692	28
53 714	408	53714.96644-15.24025	0.27381	10.071-10.478	10.2661	0.0036	0.0735	54
53 718	53	53718.93715-18.96768	0.03053	10.233-10.569	10.4005	0.0113	0.0820	48
53 719	60	53720.16045-20.20221	0.04176	10.251-10.509	10.3689	0.0082	0.0637	59
53 721	463	53721.90647-22.18562	0.27915	10.150-10.514	10.3352	0.0031	0.0665	43
53 723	419	53723.89227-24.20482	0.31255	10.510-10.854	10.6845	0.0031	0.0630	49
53 727	325	53728.01029-28.20304	0.19275	10.407-10.959	10.7631	0.0059	0.1071	48
53 728	138	53728.90736-29.15139	0.24403	10.597-11.003	10.8262	0.0065	0.0759	119
53 729	418	53729.88847-30.15052	0.26205	10.534-10.939	10.7779	0.0038	0.0779	48
53 730	467	53730.88198-31.16156	0.27958	10.596-11.038	10.8290	0.0039	0.0848	48
53 731	457	53731.87834-32.14991	0.27157	10.422-10.938	10.6882	0.0045	0.0957	48
53 733	199	53734.00208-34.14173	0.13965	10.615-11.013	10.7913	0.0053	0.0745	59
53 741	426	53741.93878-42.34369	0.40491	10.400-10.887	10.6814	0.0043	0.0886	40
53 742	490	53742.88202-43.12333	0.24131	10.378-10.933	10.6474	0.0042	0.0938	41
53 743	302	53743.88083-44.04232	0.16149	10.525-11.000	10.7455	0.0055	0.0949	41
53 753	355	53753.88591-54.07058	0.18467	10.482-10.827	10.6851	0.0035	0.0665	41
53 756	201	53756.97976-57.10862	0.12886	10.597-10.861	10.7513	0.0042	0.0590	51
53 757	428	53757.89002-58.07701	0.18699	10.582-10.836	10.7254	0.0022	0.0463	35
53 758	403	53758.89195-59.07778	0.18583	10.557-10.792	10.6759	0.0023	0.0452	26
53 759	403	53759.90846-60.08968	0.18122	10.450-10.748	10.5982	0.0033	0.0659	26
53 760	87	53760.89155-60.92635	0.03480	10.507-10.646	10.5905	0.0029	0.0269	30
53 761	199	53761.89168-61.98891	0.09723	10.540-10.846	10.6917	0.0041	0.0572	41
53 762	305	53762.92413-63.08970	0.16557	10.618-10.914	10.7826	0.0033	0.0573	45
53 767	217	53767.94171-68.05934	0.11763	10.552-10.744	10.6707	0.0027	0.0401	46
53 769	228	53769.90351-70.05308	0.14957	10.606-10.778	10.7000	0.0025	0.0381	46
53 774	177	53774.92833-75.04274	0.11441	10.548-10.748	10.6563	0.0030	0.0403	29
53 776	144	53776.90179-76.97372	0.07193	10.529-10.783	10.6487	0.0049	0.0587	35
53 777	289	53777.90157-78.05429	0.15272	10.523-10.770	10.6635	0.0029	0.0498	35
53 778	357	53778.91810-79.05101	0.13291	10.526-10.748	10.6468	0.0024	0.0462	18
53 783	298	53783.92239-84.03073	0.10834	10.289-10.590	10.4454	0.0036	0.0619	29
53 790	218	53790.91312-91.02148	0.10836	10.484-10.709	10.5921	0.0041	0.0608	40
53 792	173	53792.91504-93.02008	0.10504	10.471-10.673	10.6038	0.0025	0.0331	45
53 797	91	53797.95336-98.00170	0.04834	10.381-10.563	10.4842	0.0045	0.0432	45
53 800	171	53800.91434-00.98895	0.07461	10.513-10.709	10.6096	0.0032	0.0424	20

– 53 721−53 723: "upper limit for decay", During two days between these nights, the brightness decreased by $0\overset{m}{.}34$. Due to bad weather in the intermediate night, the time interval of 2 days represents an upper limit to the total duration of decay.
– 53 727−53 800: "post-outburst slow brightening", for which the mean slope is $\dot{m} = -0.00288(5)$ mag/day, and the values of $\bar{m}$ for individual nights can differ from the corresponding linear fit by up to $\approx 0\overset{m}{.}1$.

The observed light curves are shown in Fig. 2. They exhibit a variety of shapes and types of variability. The "3.2-h variability is occasionally prominent (e.g. 53 727, 537 41-53 762), at other date, this component of variability has a remarkably small amplitude (53 685, 53 698). The amplitude of the quasi-periodic oscillations (QPO), which were previously reported by other authors, varies from night to night and also within one partial run.

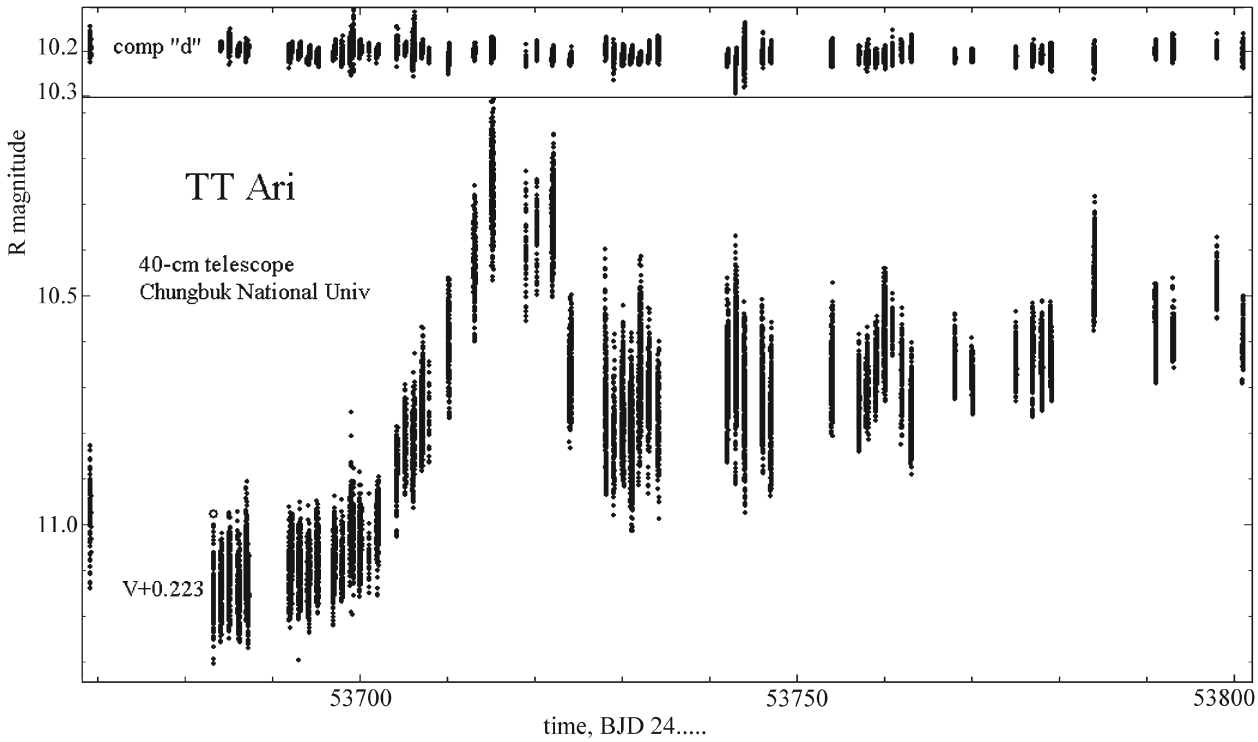

Fig. 1. The complete light curve of TT Ari for 51 nights of observations (*bottom*) and of the comparison star "d". The V magnitudes in one night (53 683) of observations were shifted using the mean value of the instrumental color index $V - R = 0\overset{m}{.}223$.

Table 3. Brightnesses of the comparison and check stars ("c" and "d", Goetz 1985) compiled from different publications.

U	B	V	R	I	Ref.
comparison star "c" = GSC 1207 1535					
12.04	11.72	11.01	10.41	9.97	Efimov et al. (1998)
11.91	11.68	10.99			Shafter et al. (1985)
"	"	"			Goetz (1985)
	11.74	11.05	10.66	10.3	Henden (2007)
	11.82	11.17			VSNET (2005)
		11.1			AAVSO (2007)
check star "d" = GSC 1207 1562					
13.38	12.17	11.02			Goetz (1985)
	12.20	11.05	10.51	9.97	Henden (2007)
	11.96	10.86			VSNET (2005)
		11.1			AAVSO (2007)

For numerical parametrization of the observed variability, we used several complementary methods of time-series analysis: periodogram, wavelet analysis, running sine and running parabola approximation, and O−C analysis, which are described below.

3.2. Wavelet analysis

The wavelet analysis is one of the most powerful methods of studying signals of variable periods and amplitudes (cf. Daubechies 1988). For the "'wavelet periodograms", we used the test functions $S(P)$, $r(P)$ (Andronov 1998a) and WWZ (Foster 1996), which are specially elaborated for a case of finite signals with possibly non-regular arguments. Their statistical properties were studied by Andronov (1998b). These test functions are complementary, although their peaks are related to effective values of the period. Their physical sense may be explained briefly as follows (see Andronov 1998a,b, for a detailed description): $r(P)$ is an effective amplitude (which is equal to a semi-amplitude, if the signal is purely sinusoidal); $S(P)$ is a weighted mean of the squared correlation coefficient, so $S(P) \approx 0$ corresponds to a poor periodic fit, and $S(P) = 1$ indicates that the period is correct (if the analyzed signal is purely sinusoidal); and WWZ is the "energy" signal-to-noise ratio, such that the false alarm "probability" FAP $\approx \exp(-\mathrm{WWZ})$.

These test functions are shown in Fig. 3 as a function of trial period P. One can discern significant scatter in the semi-amplitude $r(P)$ at small values of $\lg P (\leq -2.4$ and $\geq 0.0)$. This is an effect of the discreteness of the times of observations, and thus $r(P)$ is not the best test function as compared to the three test functions listed above. The test function $S(P)$ exhibits highest peaks at $P = 0\overset{d}{.}0143 = 20.6$ min ($\lg P = -1.844$) and $P = 0\overset{d}{.}135 = 3\overset{h}{.}24$ ($\lg P = -0.87$). The corresponding values of $S(P)$ (the mean contribution of variability at this effective period to the total variance in the signal) are remarkably similar: 0.184 and 0.182. The values of WWZ at these two optimal periods are equal to 8.0 and 25.0, respectively, so both of the proposed types of variability are statistically significant. The mean semi-amplitudes of the period are $0\overset{m}{.}0357$ and $0\overset{m}{.}0456$. The peak at $\lg P \approx 0.2$ occurs at the period, which is comparable with distance between the subsequent nights, so the effective number of points is small, and the peak is not statistically significant. So we do not interpret this timescale to be of physical nature of the object.

To study the stability of the variability parameters, the "wavelet periodograms" for individual nights are shown in Fig. 4. The range of trial periods P is restricted to between $3\Delta_{\min}$ and $t_e - t_s$, where $\Delta_{\min}$ is the time resolution (time step between subsequent observations), and $(t_e - t_s)$ is the duration of observations. Both these parameters are listed in Table 1. The peaks close to either 20.6-min, or 3.2-h show very significant night-to-night changes both in height and position.

The period determination of the 3.2-h variability is discussed in Sect. 3.6, since it exceeds the duration of many nightly runs of our observations, and it should therefore be difficult to

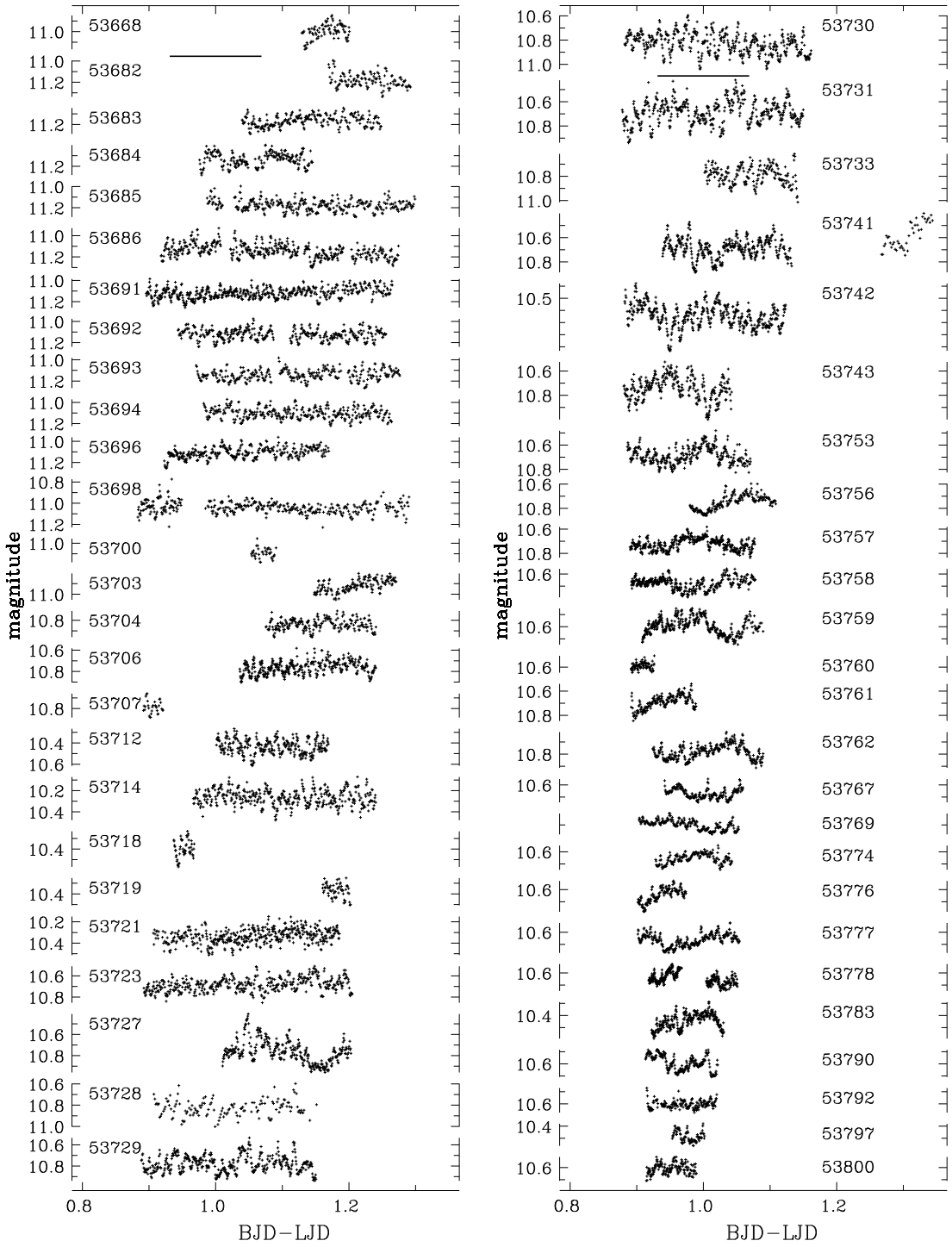

Fig. 2. The individual light curves of TT Ari. Abscissa is expressed as BJD−LJD, where the "legend Julian date" LJD (−2 400 000) is shown near each curve. As the integer part of the Julian date JD often changed during our observations, we preferred to use the value corresponding to the beginning of the night. The length of horizontal lines between the first and second light curves is equal to the orbital period.

determine from periodograms for so short individual runs because of possible large distortion in the smoothing function.

3.3. Effective characteristics of QPOs

We used the following parameters to characterize the QPOs for individual nights: the period P, semi-amplitude $r(P)$, and "effective stellar magnitude" $m_{\rm QPO}$, which correspond to the maximum of $S(P)$ in the interval $-2.4 \le \lg P \le -1.7$. This interval was chosen after examination of the mean and individual "wavelet periodograms". The parameter $m_{\rm QPO} = \bar{m} + 2.5\lg((1 + 10^{0.4*r})/(1 - 10^{-0.4*r}))$ is the magnitude estimate of the source of QPOs. The physical sense is the magnitude of the source of emission, which corresponds to brightening from the stellar magnitude $(\bar{m} + r)$ (invisible) to $(\bar{m} - r)$ (visible).

These characteristics are listed in Table 4 and shown in Fig. 5. The mean semi-amplitudes of variability range from $0\overset{\rm m}{.}0139$ (run 53 760) to $0\overset{\rm m}{.}0821$ (run 53 718), i.e. vary by

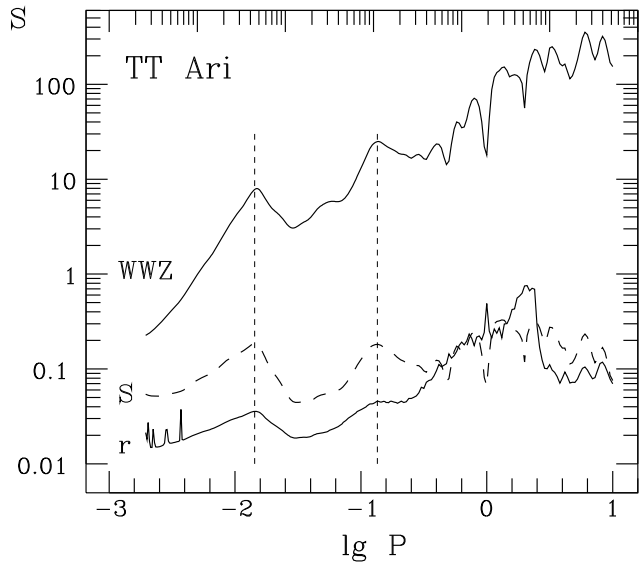

Fig. 3. The "wavelet periodograms": test functions used $S(P)$, $r(P)$, WWZ for a complete set of observations (see Andronov 1998, for a detailed description). The vertical lines mark the positions of the highest peaks at $S(f)$, which correspond to $P = 0^{\rm d}.0143 = 20.6$ min and $P = 0^{\rm d}.135 = 3^{\rm h}.24$.

a factor of 5.9. The lg P ranges from −2.13 to −1.72, apart from one night 53 760 with an outlying value of −2.36 (the run was short, so this value represents only a short time interval and therefore is not very accurate).

The time variation in $\bar{m}$ was considered earlier, by splitting the interval of our observations according to this parameter. Surprisingly, the outburst detected in $\bar{m}$ has a very different shape and duration in $m_{\rm QPO}$. At the beginning of the outburst (53 703, 53 704), as the mean brightness $\bar{m}$ started to increase, the semi-amplitude r and $m_{\rm QPO}$ are within the ranges characteristic for the "pre-outburst" stage. The values of $m_{\rm QPO}$ then range from $12^{\rm m}.85$ to $13^{\rm m}.76$ (apart from one short night 53 718) for the nights 53 706−53 753. This stage, which could be referred to as "QPO-excited", starts from the outburst rise and lasts at least $30^{\rm d}$ after the end of a $\approx 10^{\rm d}$ outburst.

After that, $m_{\rm QPO}$ steeply decreases (i.e. the QPO flux increases) with a best fit slope $dm_{\rm QPO}/dt = -0.0125(37)$ mag/day, which is far higher than that of $-d\bar{m}/dt = 0.0037(11)$ mag/day. However, night-to-night variability is significant, the slopes only slightly exceeding the "3σ-level". The best fit for 18 nights (apart from the short run 53 760) is $m_{\rm QPO} = 14^{\rm m}.05(3) + 2.61(42) \cdot (\bar{m} - 10^{\rm m}.64)$, the slope being determined to be at the far more significant 6.3σ-level. This argues for a statistically significant relationship between $m_{\rm QPO}$ and $\bar{m}$. The slope is larger than unity. In other words, with increasing mean flux, also increase other characteristics: the semi-amplitude (related to arbitrary amplitude of the flux variations), the brightness of the source of QPO (related to the flux of QPO) and the period. The statistical significance of the latter relationship at the 3.4σ-level is evident from the best fit function $\lg r = -1.628(14) + 0.40(11) \cdot (\lg P + 1.9)$.

The relations presented above were derived for the section of the light curve after the outburst of the QPO. The complete diagrams showing pairs of parameters (not presented in the paper), exhibit several groups with smaller number of points inside instead of a monotonic line with some scatter. In Fig. 6, the diagrams of $m_{\rm QPO}$, lg P, and lg r vs. $\bar{m}$ are shown. One may note two distinctly different groups at the intermediate brightness interval, which are shown by squares (4-th interval) and crosses (5-th interval). These intervals are consequent in time, and are characterized by similar ranges in $\bar{m}$. However, they differ in the values of lg r, and, therefore, in $m_{\rm QPO}$. In contrarst to the 5-th interval, there are no significant statistical dependencies on $\bar{m}$ of any of the parameters $m_{\rm QPO}$, lg P, and lg r.

Table 4. Characteristics of the highest peaks in the "wavelet periodogram" $S(P)$ for the individual nights: $\bar{t}$ – mean time of the run, $\bar{m}$ – sample mean magnitude (as in the Table 1), $m_{\rm QPO}$ – stellar magnitude of QPOs, lg P, lg r, $S(P)$.

$\bar{t}$	$\bar{m}$	$m_{\rm QPO}$	lg P	lg r	$S(P)$
53 669.16608	10.9975	13.8932	–2.06	–1.4237	0.2054
53 683.22808	11.1820	13.6733	–1.96	–1.2620	0.4162
53 684.13588	11.1667	14.1842	–1.94	–1.4724	0.2807
53 685.06281	11.1341	14.0890	–2.02	–1.4473	0.2107
53 686.14215	11.1767	14.2336	–2.01	–1.4881	0.2177
53 687.08587	11.1435	14.0220	–2.07	–1.4168	0.2456
53 692.06316	11.1194	14.2705	–2.03	–1.5258	0.2309
53 693.09523	11.1228	13.8781	–1.91	–1.3675	0.3882
53 694.12418	11.1418	13.9650	–1.99	–1.3947	0.3655
53 695.12250	11.1039	13.9996	–2.01	–1.4237	0.2942
53 697.03612	11.1090	14.3200	–1.86	–1.5498	0.1978
53 699.07330	11.0404	14.1175	–1.94	–1.4962	0.1956
53 701.07125	11.0932	13.9689	–2.04	–1.4157	0.3457
53 704.21028	10.9180	13.9387	–2.07	–1.4737	0.3039
53 705.15261	10.8413	13.9049	–1.97	–1.4908	0.2235
53 707.12664	10.7678	13.5723	–1.94	–1.3872	0.2839
53 707.90587	10.7859	12.9399	–1.98	–1.1273	0.7236
53 713.08494	10.4350	12.8533	–1.82	–1.2328	0.3574
53 715.10349	10.2661	13.0893	–1.92	–1.3947	0.1543
53 718.95241	10.4005	12.4503	–2.00	–1.0857	0.5146
53 720.18131	10.3689	13.3453	–1.98	–1.4559	0.1677
53 722.05972	10.3352	13.4575	–2.13	–1.5143	0.1299
53 724.04834	10.6845	13.7616	–1.75	–1.4962	0.1488
53 728.10643	10.7631	13.1026	–1.81	–1.2013	0.2479
53 729.01869	10.8262	13.1744	–1.80	–1.2048	0.3683
53 730.01934	10.7779	13.2913	–1.87	–1.2708	0.2663
53 731.02173	10.8290	13.1531	–1.87	–1.1952	0.3237
53 732.01320	10.6882	12.8525	–1.83	–1.1314	0.3356
53 734.07165	10.7913	13.5340	–1.90	–1.3625	0.1931
53 742.05811	10.6814	13.2361	–1.81	–1.2874	0.2354
53 743.00344	10.6474	12.9647	–1.81	–1.1925	0.3037
53 743.96000	10.7455	13.2835	–1.90	–1.2807	0.2038
53 753.97373	10.6851	13.7188	–2.02	–1.4789	0.1812
53 757.04199	10.7513	14.3629	–2.06	–1.7100	0.1480
53 757.98316	10.7254	14.3314	–2.08	–1.7077	0.1520
53 758.96880	10.6759	14.3272	–2.07	–1.7258	0.1330
53 759.98530	10.5982	13.9531	–1.96	–1.6073	0.1150
53 760.90784	10.5905	14.5697	–2.36	–1.8570	0.1606
53 761.94042	10.6917	13.9743	–1.83	–1.5784	0.1907
53 763.00687	10.7826	14.2102	–1.94	–1.6364	0.1304
53 768.00039	10.6707	14.3998	–1.93	–1.7570	0.1229
53 769.97754	10.7000	14.0952	–1.74	–1.6234	0.3257
53 774.98545	10.6563	14.1222	–1.93	–1.6517	0.2238
53 776.93634	10.6487	13.9733	–2.01	–1.5952	0.1824
53 777.97625	10.6635	14.2261	–2.09	–1.6904	0.1596
53 778.97798	10.6468	14.1078	–1.89	–1.6498	0.1498
53 783.97776	10.4454	13.5259	–1.84	–1.4976	0.1797
53 790.96543	10.5921	13.7395	–1.72	–1.5243	0.1516
53 792.97117	10.6038	14.0844	–1.87	–1.6576	0.2388
53 797.97754	10.4842	13.5245	–1.73	–1.4815	0.2869
53 800.95004	10.6096	14.0419	–1.72	–1.6383	0.1495

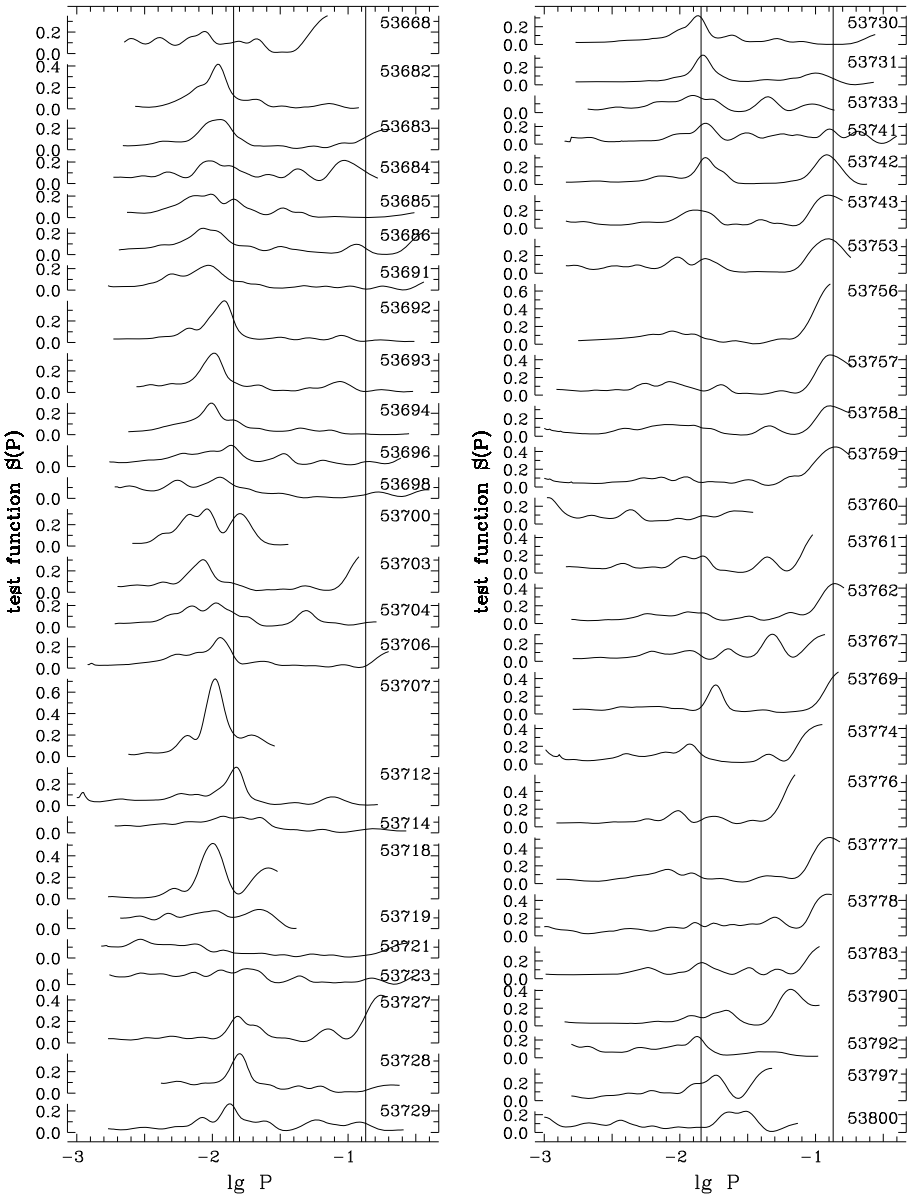

Fig. 4. The individual wavelet periodograms $S(P)$ for all nights of observations. To avoid bias, the curves are shown in a range of trial periods from $3\Delta_{\rm min}$ to $t_{\rm e} - t_{\rm s}$ (see Andronov 1998, for a detailed description). The vertical lines mark the positions of the highest peaks of $S(f)$ for the complete set of observations, which correspond to $P = 0\overset{\rm d}{.}0143 = 20.6$ min and $P = 0\overset{\rm d}{.}135 = 3\overset{\rm h}{.}24$. The 5-digit "legend Julian date" LJD is close to each graph.

These relations will provide important tools for future modeling of accretion disks with slowly increasing brightness.

3.4. QPO period variability during observational runs

Drastic variability in the nightly values of QPO characteristics is observed. To study this phenomenon, we used the wavelet test function $S(f)$ (Andronov 1998a,b), since the position of peaks for this function coincides with the underlying period. The dependence of $\lg P$ on time for all individual nights is shown in Fig. 7. Due to the stability of the periods during the run, one can distinguish between nights of small period variations (e.g. 53 712) and multiple switches (e.g. 53 691). These apparent switches in the $P(t)$ diagrams can be explained by aperiodic flares or dips, which occasionally alter the interval between the brightness maxima or minima, respectively. One may neglect switches at the borders of observations, since the trial fit used in the wavelet analysis is filled with observations extremely asymmetrically, which produces larger statistical errors and an apparent rise or decay in smoothing signal. Examples of these jumps in frequency in the "negative superhump" state in 1989 were reported by Kraicheva et al. (1999).

3.5. Search for possible periodic components

The presence of QPOs does not imply that there are no truly periodic variations, e.g. related to the spin period of the white dwarf. A similar situation is present in the magnetic dwarf nova DO Dra, where the new phenomenon – "transient periodic oscillations" dominates over the spin variability (Andronov et al. 2008). For this purpose, we used the program "Fo", which completes a periodogram analysis based on a least squares cosine fit (Andronov 1994). The test function $S(f)$ is a square of the correlation coefficient between the "observed" and "computed" (using the least squares sine fit for a trial frequency) values. The statistical significance of the peak increases with its height (see Andronov 1994, for a description of the statistical properties of this test function).

The low frequency "$3\overset{\rm h}{.}2$" component has a significant amplitude, which causes a bias in the periodogram. To decrease this bias, it is needed to remove this type of variability from the

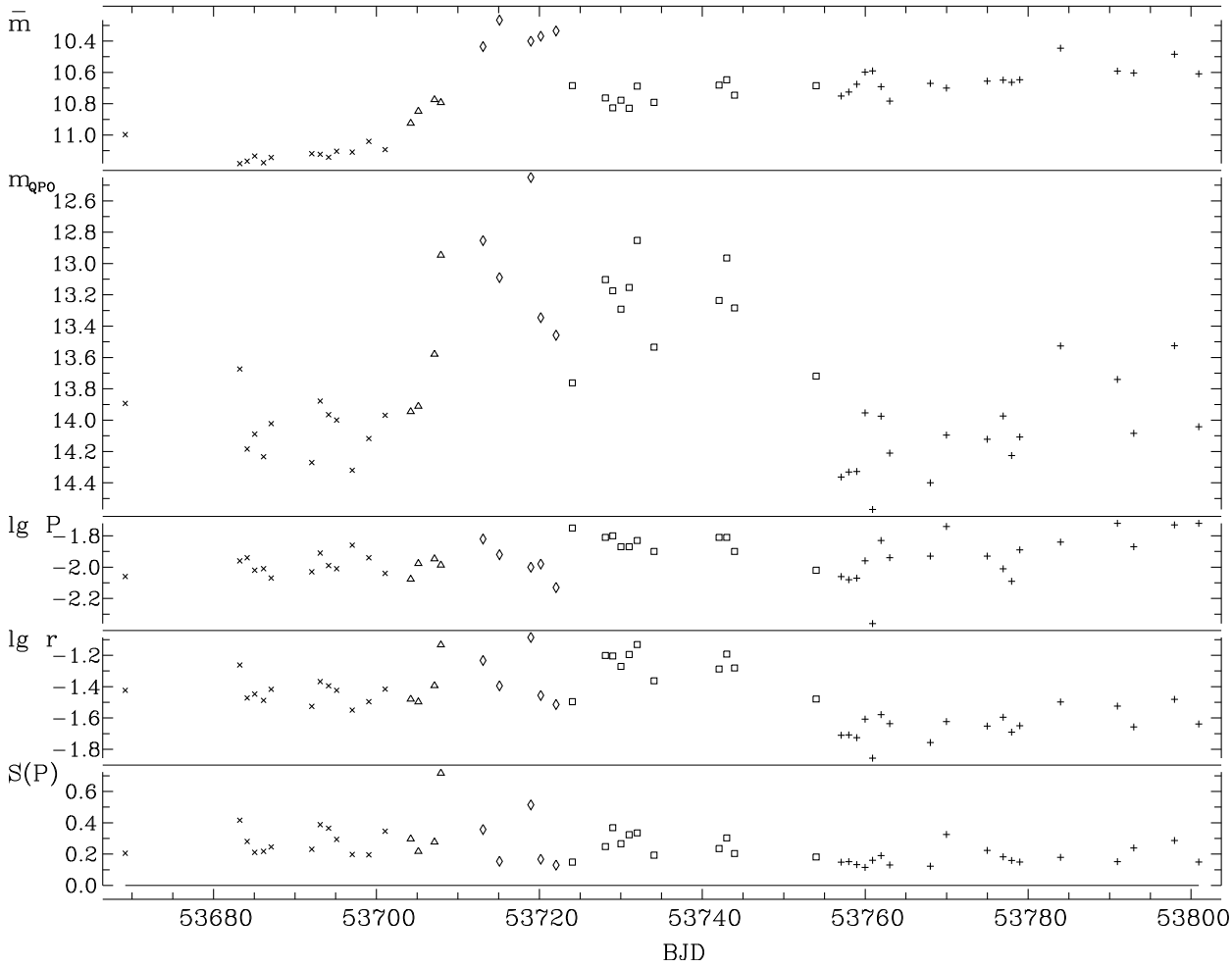

Fig. 5. Dependence of the characteristics of individual runs on time: sample mean magnitude $\bar{m}$, effective magnitude of the source of the QPOs $m_{\rm QPO}$, logarithm of period lg P of QPOs, logarithm of semi-amplitude lg r of QPOs. and the corresponding test function $S(P)$. Each point represents one night.

original observations before the periodogram analysis. Similar to BG CMi (Kim et al. 2005) and DO Dra (Andronov et al. 2008), we used the "running sine" (RS) fit, with an initial period $P = 0\overset{\rm d}{.}01413$, taken from the wavelet periodogram. Generally, the characteristics of this fit (not shown) confirm our previous result – variability in the period and semi-amplitude. We therefore used only an estimate of the low-frequency trend to compute the residuals of the signal from the smoothing values (O−C).

The test function $S(f)$ for the residuals (O−C) is plotted versus frequency in cycle/day. For reference, the frequency, which corresponds to the most likely period for the mean wavelet periodogram, is 69.8 cycles/day. The individual periodograms are shown in Fig. 8. During some nights, the peaks were high and narrow (e.g. 53 692, 53 731, 53 769), which corresponded to oscillations, which were stable during the night. Wide peaks are often high (53 700, 53 707, 53 718) and broad, which is consistent with the peak width being inverse proportional to the duration of observations. The periodograms show multiple peaks (e.g. 53 668), which correspond to the absence of stability in the periods during the nights. The frequency corresponding to the highest peak is a reliable parameter for QPOs. However, due to period changes, the highest peak may not correspond to that of the "wavelet periodogram" $S(P)$, and the estimate of the semi-amplitude r is far smaller than that for the wavelet (they coincide only, if the signal is strictly periodic). Thus we decided to use estimates from the wavelet analysis. The periodogram for all nights (not shown because of a huge length of the file) shows its highest peak at the frequency $f = 68.2712(3)$ (period $P = 0\overset{\rm d}{.}0146475(6) = 21.0924$ min, semi-amplitude $r = 0\overset{\rm m}{.}107(6)$, and initial epoch for the maximum brightness at $T_{\rm max} = 53\,731.73880(14)$). Although $S(f) = 0.02$ is small, i.e. only two per cent of the variability may be explained by this periodic component, the "false alarm probability" FAP $= 10^{-56.3}$ is very low, indicating that this variability is statistically significant.

The estimate of the semi-amplitude is far smaller than that of the wavelet analysis, so this peak may be a sum of peaks from several nights with QPOs with similar frequency.

3.6. Superhump period

Since the system exhibits several types of variability, the determination of the period is complicated. Due to the outburst and mean brightness fluctuations, the slow variations are not periodic. They affect results of the periodogram analysis, so a preliminary removal of these variations from the original data is needed. In an addition, the light curve sometimes exhibits two maxima during the "$3\overset{\rm h}{.}2$-h" period, which was preliminary suggested. Following an approach used during our previous campaigns (Tremko et al. 1996; Andronov et al. 1999), we used the

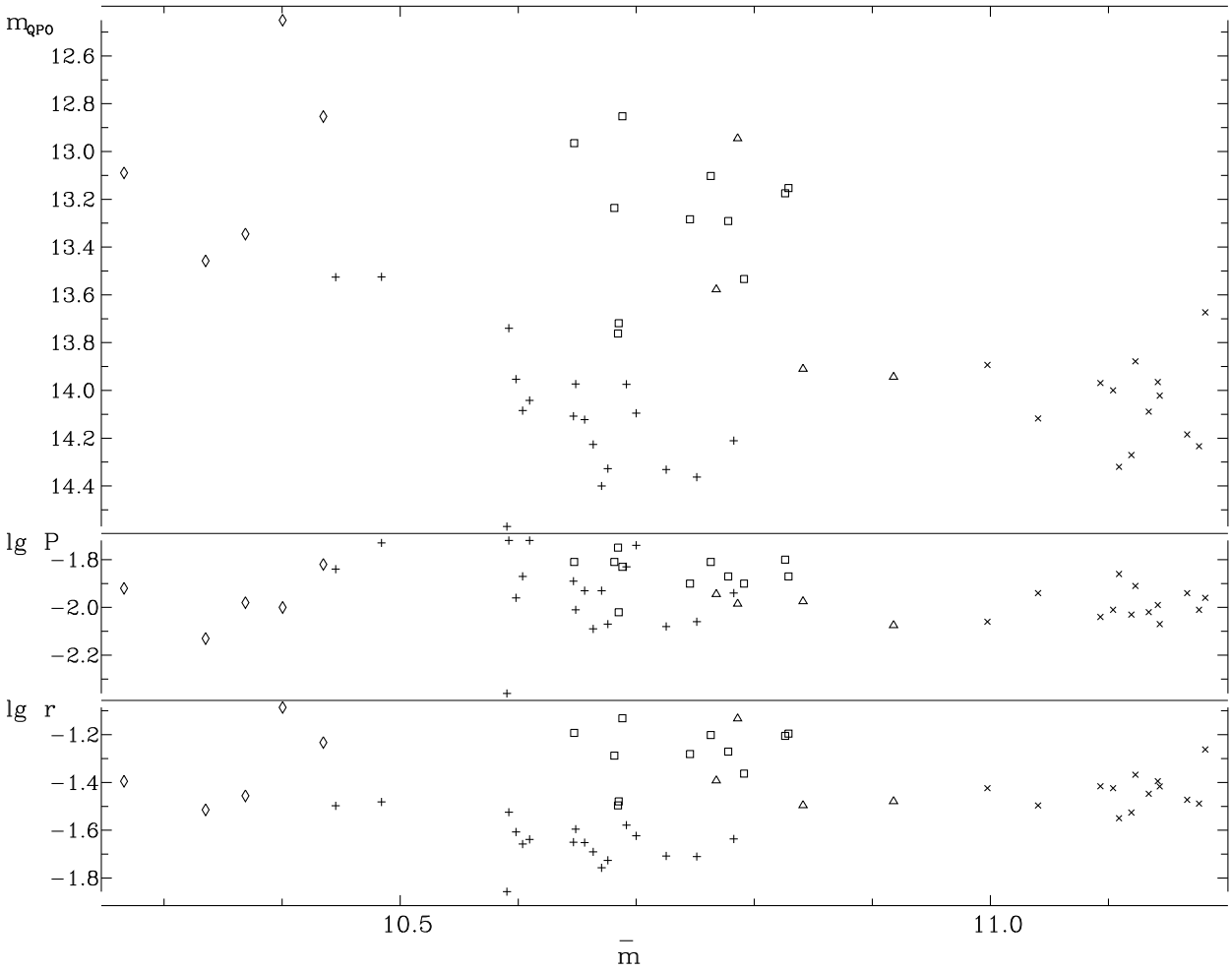

Fig. 6. Dependence on $\bar{m}$ of the characteristics of individual runs: effective magnitude of the source of the QPOs ($m_{\rm QPO}$), and logarithm of period (lg P) of QPOs, and logarithm of semi-amplitude (lg r) of QPOs. Each point corresponds to one night.

times of prominent minima of the light curve. For better statistical accuracy, we used the method of "asymptotic parabola" (Marsakova & Andronov 1996). The list of 12 minima is presented in Table 5.

In seaching for possible periods, we analyzed the 12 minima timings. The program "PerMin" was used, which applies the "method of characteristic events" (Andronov 1991). In this method, two parameters (period and initial epoch) are determined, which correspond to a minimum of the rms deviation of phases from zero. The corresponding dependence of the test function $\sigma(P)$ on the trial period is shown in Fig. 9.

The best fit function elements were:

$$T_{\rm min} = {\rm BJD2\,453\,747.0700(47)} + 0.13232(5) \cdot E. \qquad (1)$$

The period value was close to that published for previous campaigns: $P = 0\overset{\rm d}{.}132959(13)$ (Tremko et al. 1996) and $0\overset{\rm d}{.}133160(4)$. The difference between the pairs of period values exceeds the statistical errors, but all these values are much smaller, than in the "positive superhump" state $P = 0\overset{\rm d}{.}14926$ (Skillman et al. 1998) or $0\overset{\rm d}{.}14840$ (Andronov et al. 2005). During our set of observations, the star was therefore in the "negative superhump" state.

The deviations in the phases from zero sometimes reached 0.2, which prevented these minima to be interpreted by periodic eclipses. We tried to find a better ephemeris by avoiding some of the minima (assuming that they are due to other variations), but it has not resulted in better coincidence of phase curves for all nights.

The phase light curves smoothed using the method of "running parabola" (Andronov 1997) are shown in Fig. 10. The time is expressed as a continuously increasing phase computed using the ephemeris (1), i.e. from −1 to 3, not as usually defined from 0 to 1. The brightness variability is practically shown *versus* time (divided by the period) and shifted by some integer number. In TT Ari, the instability of the phase light curve is evident not only from night to night, but also from one cycle of variability to another. This presentation of the light curve is therefore preferred, similarly to that used for the intermediate polars (e.g. Kim et al. 2005).

The filter half width is $\Delta t = 0\overset{\rm d}{.}05$, the value adopted by both Tremko et al. (1996) and Andronov et al. (1999). The positions of many minima, which were not so prominent, and therefore not listed in the Table 5, are in good agreement with the ephemeris presented above. However, for other nights, at phase zero, a secondary minimum or even a maximum may be observed. The light curves may be classified as "one-maximum" or "two-maxima" per period.

This result could be explained by significant variations in the disk luminosity, possibly due to the inhomogeneity.

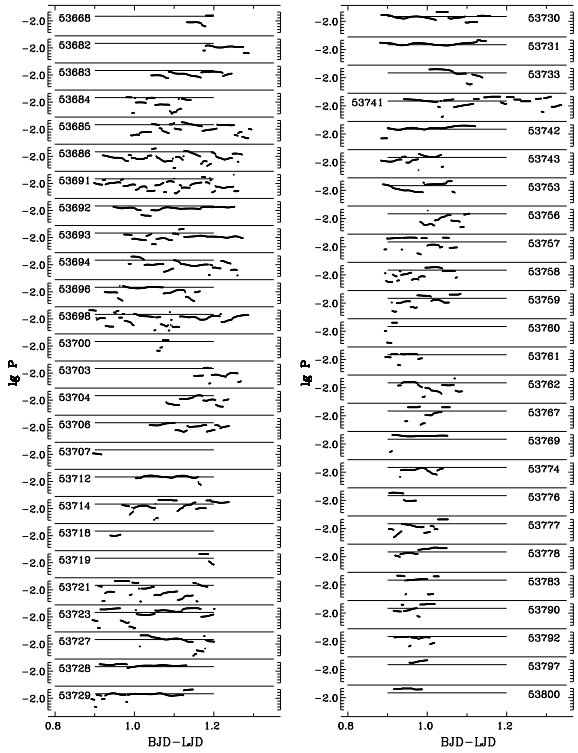

Fig. 7. Dependence of the local value of period P of the quasiperiodic oscillations (QPO), which corresponds to a highest maximum of the test function WWZ in the adopted interval $-2.4 \le \lg P \le -1.7$, for the individual nights of observations. The short horizontal lines mark the value of $\lg P = -1.844$, which corresponds to the maximum of the wavelet periodogram $S(P)$ for all data. The ordinate is marked from −2.4 to −1.7 for all nights. The 5-digit "legend Julian date" LJD is shown close to each graph. Time is expressed as BJD−LJD, as in Fig. 2.

Table 5. Characteristics of the prominent minima of the "3.2"-h variability determined using the method of "asymptotic parabola" (Marsakova & Andronov 1996): time BJD (and its error) and value of the signal $m_{\min}$ (and its error).

t, BJD	$\sigma[t]$	$m_{\min}$	$\sigma[m_{\min}]$
53 728.15648	0.00180	10.911	0.014
53 730.01153	0.00065	10.860	0.009
53 732.00013	0.00122	10.746	0.009
53 742.01621	0.00078	10.854	0.014
53 742.94917	0.00234	10.782	0.019
53 744.00722	0.00220	10.896	0.023
53 753.95263	0.00001	10.743	0.007
53 757.00094	0.00140	10.846	0.005
53 757.94716	0.00072	10.794	0.008
53 758.05255	0.00162	10.784	0.010
53 758.97022	0.00248	10.747	0.008
53 760.04089	0.00030	10.704	0.005

4. Conclusions

We present the following conclusions based on the analysis of 51 observational runs (JD 2 453 669−2 453 800), which were obtained at the 40-cm telescope of the Chungbuk National University (Korea) over 226 h:

– During the period of observations, TT Ari was in the "negative superhump" state. The preceding "positive superhump" lasted from 1996 to 2004.

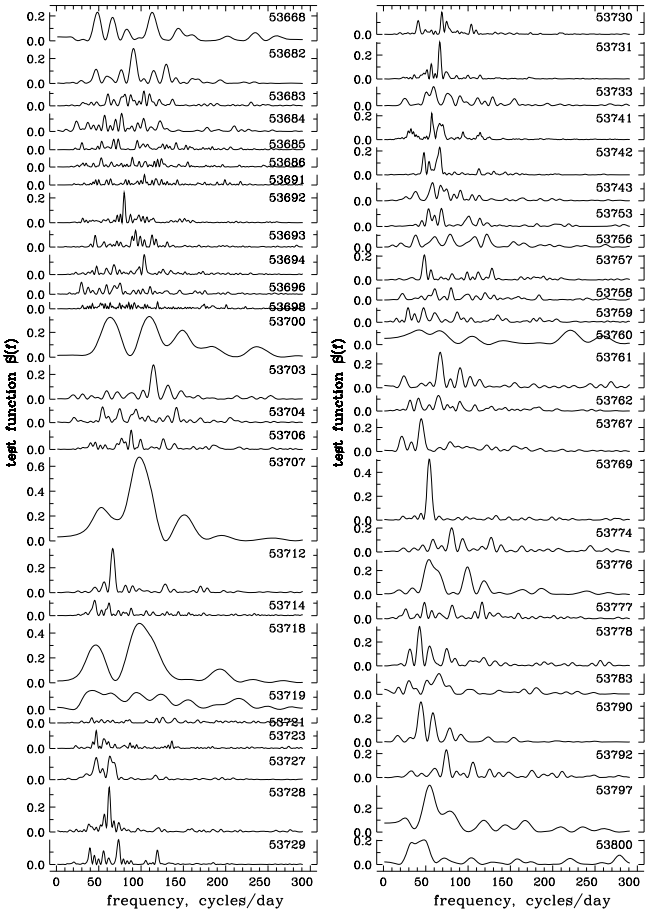

Fig. 8. The periodograms $S(f)$ for the individual runs. The 3.2-h cyclical trend was removed using the "running sine" method. The 5-digit "legend Julian date" LJD is shown close to each graph.

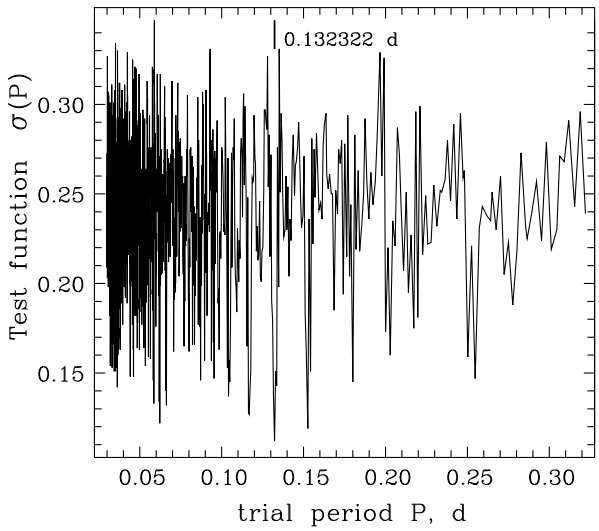

Fig. 9. The dependence of the test function $\sigma(P)$ computed for 12 selected moments of minima on the trial period P. The position of the lowest minimum at $P = 0^{\rm d}.132322$ is shown by the short line.

– As in the previous "negative superhump" states, the light curve was characterized by a "3.2-"h variability and superimposed quasi-periodic oscillations. The shape of the "superhump" curve is highly variable, showing a one-maximum (per period) or two-maxima structure.

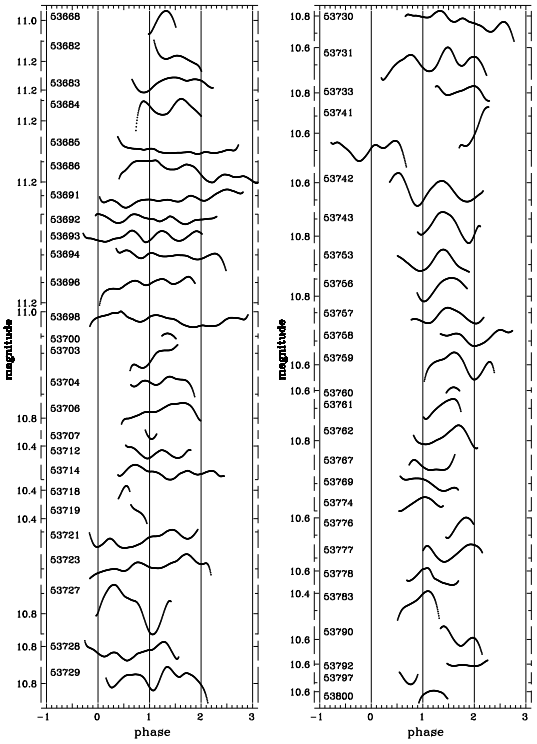

Fig. 10. Fits for individual nights using the method of running parabola with the filter half-width $\Delta t = 0^{d}.05$. The time is expressed as a continuously increasing phase computed using the ephemeris (1). The 5-digit "legend Julian date" LJD is shown near each graph.

- The ephemeris for the 12 most pronounced "superhump" minima is $T_{\min}$ = BJD 2 453 747.0700(47) + 0.132322(53)E. This is in the range detected by previous studies for the "negative superhumps". The wide range of minima phases (from −0.2 to 0.2) indicates that these minima may not represent eclipses of the emission source, which is fixed in the rotating frame, but the position may instead be dynamically variable. Another source of the "superhump" light-curve distortion (and, consequently, of the phase scatter) is a strong flickering or aperiodic small-amplitude flares.
- The quasi-periodic oscillations (QPO) are present with a mean "period" of 21.6 min and mean semi-amplitude of 36 mmag. The position and height of the peaks at the "wavelet periodogram" vary from night to night and occasionally during the night.
- The dependence on either time, or mean brightness, of the magnitude of the source of QPOs, the period, and the amplitude indicates that the interval of observations is to be divided into 5 parts, showing different characteristics, namely: 1) the "pre-outburst" stage; 2) the "rise to outburst"; 3) "top of the outbursts"; 4) "post-outburst QPO" state; and 5) "slow brightening". The new phenomenon was detected, which we called the "post-outburst QPO" state. This state was characterized by a large amplitude of QPOs for more than 30 days ("4") after the outburst (part "3") lasting 10 days. During both states "3" and "4", the amplitude of the QPOs was larger, than in the states "1" and "5". The photometric behavior of the system was therefore dependent on the current mean magnitude, and also the previous state.
- The analysis of pairs of characteristics for these groups separately indicated statistically significant correlations only for the state "5". For this state, the period, amplitude and brightness of the source of QPOs also increase with increasing mean brightness.
- During the present stage of "negative superhumps" the brightness varied between $10^{m}.27$ and $11^{m}.18$, whereas the mean brightness in the "positive superhump" state was only slightly smaller: $R \sim 11^{m}.3$ (Andronov et al. 2004). This implies that even small variations in mean brightness (few tenth of magnitude) are sufficient to switch between "positive" and "negative" superhumps. "Positive" superhumps are excited at lower luminosity, than the "negative" ones. Since TT Ari occasionally exhibits low states of $\approx 17^{m}$, it will be an interesting observational task to study the type of variability that dominates in the low luminosity state.

Acknowledgements. This work was supported by the Korea Research Foundation Grant funded by the Korean Government (MOEHRD, Basic Research Promotion Fund) (KRF-2007-C00121-I00511) and was partially supported by the Ministry of Education and Science of Ukraine.

References

Andronov, I. L. 1991, KFNT, 7, 2, 78
Andronov, I. L. 1994, Odessa Astron. Publ., 7, 49 http://il-a.pochta.ru/oap7_049.pdf
Andronov, I. L. 1997, A&AS, 125, 207
Andronov, I. L. 1998a, KFNT, 14, 490
Andronov, I. L. 1998b, in Self-Similar Systems, Dubna, 57-70, http://il-a.pochta.ru/dubna.pdf
Andronov, I. L., Arai, K., Chinarova, L. L., et al. 1999, AJ, 117, 574
Andronov, I. L., Burwitz, V., Chinarova, L. L., et al. 2005, IBVS, 5664, 1
Andronov, I. L., Chinarova, L. L., Han, W., Kim, Y., & Yoon, J.-N. 2008, A&A, 486, 855
Bailey, J. 1975, J. Brit. Astr. Assoc., 86, 30
Bianchini, A. 1990, AJ, 99, 1941
Daubechies, I. 1988, Ten Lectures on Wavelets (Cambridge Univ. Press)
Efimov, Yu. S., Shakhovskoy, N. M., Andronov, I. L., & Kolesnikov, S. V. 1998, BCrAO, 94, 215
Foster, G. 1996, AJ, 112, 1709
Goetz, W. 1985, IBVS, 2823, 1
Hellier, C. 2000, NAR, 44, 131
Hellier, C. 2001, Cataclysmic Variable Stars. How and why they vary (Berlin: Springer)
Henden, A. 2007, ftp://ftp.aavso.org/public/calib/ttaribvri.dat
Hoard, D. W. 2007, http://spider.ipac.caltech.edu/staff/hoard/biglist.html
Hollander, A., & van Paradijs, J. 1992, A&A, 265, 77
Hudec, R., Huth, H., & Fuhrmann, B. 1984, Obs, 104, 1
Jameson, R. F., Sherrington, M. R., King, A. R., & Frank, J. 1982, Nature, 300, 152
Kim, Y. G., Andronov, I. L., Park, S. S., & Jeon, Y. B. 2005, A&A, 441, 663
Kozhevnikov, V. P. 1986, ATsir, 1455, 5
Kraicheva, Z., Stanishev, V., Genkov, V., & Iliev, L. 1999, A&A, 351, 607
Krautter, J., Vogt, N., Klare, G., et al. 1981, A&A, 98, 27
Leach, R., Hessman, F. V., King, A. R., Stehle, R., & Mattei, J. 1999, MNRAS, 305, 225
Massey, P., & Davis, L. E. 1992, A User's Guide to Stellar CCD Photometry with IRAF (Tucson: NOAO)
Mardirossian, F., Mezzetti, M., Pucillo, M., et al. 1980, A&A, 85, 29
Marsakova, V. I., & Andronov, I. L. 1996, Odessa Astron. Publ., 9, 127 http://oap09.pochta.ru
Neckel, Th., & Chini, R. 1980, A&AS, 39, 411
Semeniuk, I., Schwarzenberg-Czerny, A., Duerbeck, H., et al. 1987, AcA, 37, 197
Shafter, A. W., Szkody, P., Liebert, J., et al. 1985, ApJ, 290, 707
Skillman, D. R., Harvey, D. A., Patterson, J., et al. 1998, ApJ, 503, 67L
Stanishev, V., Kraicheva, Z., & Genkov, V. 2001, A&A, 379, 185
Stetson, P. B. 1987, PASP, 99, 191
Tremko, J., Andronov, I. L., Chinarova, L. L., et al. 1996, A&A, 312, 121
Warner, B. 1995, Cataclysmic Variable Stars (Cambridge Univ. Press)
Welsh, W. F., & Martell, Ph. J. 1996, MNRAS, 282, 739
Wenzel, W., Bojak, W., Critescu, C., et al. 1986, Preprint Astron. Inst. Czechoslovak Acad. Sci., 38, 44
Yoon, J. N., Andronov, I. L., Cha, S. M., Chinarova, L. L., & Kim, Y. G. 2006, ATel, 718, 1